IOPscience iopscience.iop.org

Home Search Collections Journals About Contact us My IOPscience

Two-band ferromagnetic Kondo-lattice model for local-moment half-metals

This article has been downloaded from IOPscience. Please scroll down to see the full text article.

2008 J. Phys.: Condens. Matter 20 035222

(http://iopscience.iop.org/0953-8984/20/3/035222)

View the table of contents for this issue, or go to the journal homepage for more

Download details:
IP Address: 129.252.86.83
The article was downloaded on 29/05/2010 at 07:26

Please note that terms and conditions apply.

J. Phys.: Condens. Matter **20** (2008) 035222 (6pp) doi:10.1088/0953-8984/20/03/035222

Two-band ferromagnetic Kondo-lattice model for local-moment half-metals

M Kreissl and W Nolting

Humboldt-Universität zu Berlin, Institut für Physik, Lehrstuhl Festkörpertheorie, Newtonstrasse 15, 12489 Berlin, Germany

E-mail: kreissl@nld.ds.mpg.de

Received 26 September 2007, in final form 12 November 2007
Published 19 December 2007
Online at stacks.iop.org/JPhysCM/20/035222

Abstract

We introduce a two-band Kondo-lattice model to describe ferromagnetic half-metals with local magnetic moments. In a model study, the electronic and magnetic properties are presented by temperature-dependent magnetization curves, bandstructures, spin polarizations and plasma frequencies. These are obtained from numerically evaluated equations, based on the single-electron Green functions. We show that the mutual influence between the itinerant electrons and the local magnetic moments is responsible for several phase transitions of the half-metals, namely first and second order magnetic phase transitions, as well as half-metal to semiconductor and half-metal to semimetal transitions.

(Some figures in this article are in colour only in the electronic version)

1. Introduction

Half-metals will play the key role in spintronics [1], as do semiconductors in current electronics. Unlike semiconductors, however, the Fermi level in ideal half-metals lies in a gap between valence and conduction bands only for one spin direction, whereas for the other spin direction the bands overlap. Thus the electrical current is exclusively due to spin polarized charge carriers, with promising consequences when exploiting the spin degree of freedom in logical devices. In semimetals, valence and conduction bands overlap regardless of the spin direction, leading to unpolarized currents.

The investigation of half-metallic ferromagnets started with density functional theory calculations by de Groot *et al* [2] on the Heusler alloy NiMnSb. Subsequently, other materials were identified as half-metals, e.g. other Heusler alloys such as (Pt, Fe, Co)MnSb [3], ferromagnetic oxides like CrO_2 [4] and Fe_3O_4 [5] and colossal magnetoresistance (CMR) systems like $La_{1-x}Sr_xMnO_3$ [6].

There are no pure elements which are half-metallic ferromagnets. The classical ferromagnets Co and Ni have fully polarized 3d-states at the Fermi edge, but there are also 4s-states at E_F preventing a fully polarized current. A mechanism must be found either to push the bottom of the 4s-band above the Fermi edge or to press the latter below the band bottom. This is done by alloying or by forming an oxidic compound. Thus all known half-metallic ferromagnets contain more than one element.

An important issue is the explanation of the gap, the origin of which is as equally diverse as the origin of half-metallicity. First-principles bandstructure calculations [2, 7] predict such a gap at $T = 0$. What is the physical reason for this and what happens at finite temperature? Magnon and phonon effects may give rise to a depolarization so that strict half-metallicity appears to be limited to $T = 0$.

In this paper we would like to model a local-moment half-metal to understand the basic physics of the gap behavior. Candidates for such local-moment half-metals are the CMR manganites, diluted ferromagnetic semiconductors such as $Ga_{1-x}Mn_xAs$ [8, 9] and even concentrated ferromagnetic semiconductors such as EuS [9]. We will describe these materials by a two-band Kondo-lattice model. This model (also known as an sf model) describes the mutual influence of two well-defined subsystems, localized magnetic moments stemming from a partially filled electron shell (e.g. 4f) and itinerant electrons in a partially filled energy band. Both subsystems are coupled by an on-site interband exchange interaction. One well-known consequence of this mutual influence is the carrier-induced (anti)ferromagnetism in the local-moment subsystem (Rudermann–Kittel–Kasuya–Yosida, RKKY), and another is the striking temperature dependence of the bandstates resulting, for example, in a red shift of the band bottom upon cooling below T_C [10, 11].

To describe local-moment half-metals we apply a two-band Kondo-lattice model (the principle is depicted in figure 1). The itinerant electrons belong to a conduction

 © 2008 IOP Publishing Ltd Printed in the UK

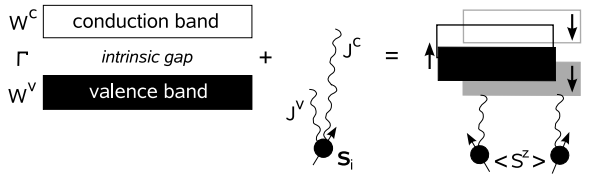

Figure 1. From left to right: free system ($J = 0$) with the electronic parameters of bandwidths W^v and W^c for valence and conduction bands, respectively, and intrinsic band gap Γ; on-site sf-coupling $J^v < 0$ and $J^c > 0$ of the valence and conduction electrons with the local-moments $\boldsymbol{S}_i$; half-metal with spin polarized electrons at the Fermi edge and mean magnetization $\langle S^z \rangle$ of the local-moments

and a valence band. For simplicity both are considered s-bands. They are exchange coupled to a system of localized magnetic moments. The exchange coupling is ferromagnetic ($J^c > 0$) for conduction electrons and antiferromagnetic ($J^v < 0$) for valence electrons. We demonstrate how the temperature dependence of the bandstates can lead to a half-metallic groundstate with a transition to semimetallic or semiconducting behavior with increasing temperature. In a mean-field picture this is simply due to the fact that upon cooling, the spin-up conduction band is energetically shifted downwards and the spin-up valence band upwards, due to interband exchange between the itinerant charge carriers and the localized moments. This results in an increased concentration of spin-up electrons. The opposite happens to the spin-down electrons. We investigate this important phenomenon in terms of the local-moment magnetization and the electron spin polarization, and try to explain it via the special behavior of the quasiparticle bandstructure.

In previous studies [12–16], single-band Kondo-lattice models were used to describe half-metals. In this paper we investigate the two-band Kondo-lattice model we have already proposed in [17] to study the electronic properties of EuB_6. Now we extend the analytical methods using the modified RKKY approach [11], which allows us to calculate the magnetic properties self-consistently instead of considering the net magnetization as a parameter following the Brillouin function. Furthermore, the focus of this paper lies in the exploration of characteristics of the introduced model and the prediction of possible properties of local-moment half-metals. This is done in a general model study rather than a specific case study.

In the next section we introduce the model and outline the theory we used for solving the underlying many-body problem. The third section is then for a detailed discussion and interpretation of the results, followed in the last section by some conclusions.

2. Theory

The proposed two-band Kondo-lattice model for half-metals describes the electronic and magnetic systems which mutually influence each other. The free electronic system (left picture in figure 1) consists of two s-bands with widths W^v and W^c of the valence and conduction bands, respectively. Between these bands we consider an intrinsic band gap Γ. As discussed above, when switching on the magnetic interaction J between the spins of the electrons in the bands and the local magnetic moments $\boldsymbol{S}_i$ (figure 1, middle picture), the bands will shift spin-dependently and form the half-metal (figure 1, right picture).

2.1. Hamiltonian

We describe the two-band Kondo-lattice model for local-moment half-metals by the following Hamiltonian:

$$H_{\mathrm{sf}} = \sum_{b}^{v,c} \left[\sum_{ij\sigma} \left(T_{ij}^{b} - \mu \delta_{ij} \right) a_{i\sigma}^{b\dagger} a_{j\sigma}^{b} - J^{b} \sum_{i} \boldsymbol{S}_i \cdot \boldsymbol{s}_i^{b} \right]. \quad (1)$$

- The index b stands for valence (v) and conduction band (c), i and j are different lattice sites and $\sigma = \uparrow$ or $\downarrow$ is the spin index of the electrons. $a_{i\sigma}^{b}$ and $a_{i\sigma}^{b\dagger}$ are the annihilation and creation operators, respectively. The chemical potential μ will be chosen to result in equal hole and electron concentrations.
- The first term of the Hamiltonian (1) is the kinetic part. T_{ij}^{b} represent the hopping integrals of the electrons and are connected to the Bloch energies $\varepsilon_{\boldsymbol{k}}$ in reciprocal space by Fourier transformation $T_{ij}^{b} = N^{-1} \sum_{\boldsymbol{k}} \varepsilon_{\boldsymbol{k}}^{b} \mathrm{e}^{\mathrm{i}\boldsymbol{k}\cdot\boldsymbol{R}_{ij}}$. For the Bloch energies we use the simple cubic, tight-binding energy dispersion [18]

$$\varepsilon_{\boldsymbol{k}}^{b} = z_b \left\{ \frac{\Gamma}{2} - \frac{W^b}{6} \left[\cos(k_x a) + \cos(k_y a) + \cos(k_z a) \right] \right\}, \quad (2)$$

  where k is the wavevector, a the lattice constant and $z_b = \delta_{bc} - \delta_{bv}$ the band sign operator. The dispersion relations (2) can be recognized in the rigidly shifted spin-down valence band and spin-up conduction band in the top-most panels of figure 3.
- The second term of the Hamiltonian (1) describes the on-site magnetic sf-coupling between the spins of the itinerant band electrons $\boldsymbol{s}_i^{b}$ and the spin of the local-moments $\boldsymbol{S}_i$. The coupling strength is $J = J^c = -J^v$, as already discussed above.

2.2. Single-electron Green functions

For the solution of the many-body problem the Green functions method is used. From the Hamiltonian (1) we can formally derive the single-electron Green functions

$$G_{k\sigma}^{b}(E) = \frac{\hbar}{E - \varepsilon_{\boldsymbol{k}}^{b} + \mu - \Sigma_{\sigma}^{b}(E)}, \quad (3)$$

where $b = v, c$ stands again for the valence and conduction bands, respectively. The single-electron Green functions (3) are written down by use of the electron self-energy $\Sigma_{\sigma}^{b}(E)$. Further details about the derivation of the self-energy for the Kondo-lattice model can be found in [19, 20]. The interpolating self-energy approach [19] is sufficient for the case of half-metals, since we are only dealing with low itinerant carrier densities.

For the low occupied conduction band, the self-energy from [19] is used

$$\Sigma_\sigma^c(E) = M_\sigma^c + \left(\tfrac{1}{2}J^c\right)^2 \frac{\alpha_\sigma G_0^c\left(E + M_\sigma^c\right)}{1 - \frac{1}{2}J^c G_0^c\left(E + M_\sigma^c\right)}, \tag{4}$$

with the abbreviation $\alpha_\sigma = S(1+S) - z_\sigma\langle S^z\rangle(1 + z_\sigma\langle S^z\rangle)$, the spin sign operator $z_\sigma = \delta_{\sigma\uparrow} - \delta_{\sigma\downarrow}$, the mean magnetization $\langle S^z\rangle$, the free propagator $G_0^b(E) = N^{-1}\sum_{\boldsymbol{k}}\hbar(E - \varepsilon_{\boldsymbol{k}}^b + \mu)^{-1}$ and what would be the mean-field result for the self-energy $M_\sigma^b = -\frac{1}{2}J^b z_\sigma\langle S^z\rangle$.

For the valence band we also have a low concentration of itinerant carriers, the holes. The self-energy from [19] needs some adaptation using the electron–hole symmetry. This was done previously in [17] and leads to the electron self-energy for the valence band

$$\Sigma_\sigma^v(E) = M_\sigma^v + \left(\tfrac{1}{2}J^v\right)^2 \frac{\alpha_{-\sigma} G_0^v(E + M_\sigma^v)}{1 + \frac{1}{2}J^v G_0^v(E + M_\sigma^v)}. \tag{5}$$

With the self-energies (4) and (5) the Green functions (3) for valence and conduction bands can now be determined.

2.3. Electronic properties

The knowledge of the Green functions allows the calculation of the spectral density

$$S_{\boldsymbol{k}\sigma}^b(E) = -\frac{1}{\pi}\,\mathrm{Im}\; G_{\boldsymbol{k}\sigma}(E) \tag{6}$$

for any wavevector $\boldsymbol{k}$. Evaluated for wavevectors along the standard symmetry points of the first Brillouin zone equation (6) leads to the quasiparticle bandstructure presented in the next section.

Furthermore, we will present the spin polarization of the conduction electrons

$$P = \frac{n_\uparrow - n_\downarrow}{n_\uparrow + n_\downarrow}, \tag{7}$$

with the spin-dependent electron density

$$n_\sigma = \sum_{\boldsymbol{k}} \int f_-(E) S_{\boldsymbol{k}\sigma}^c(E)\,\mathrm{d}E \tag{8}$$

and the plasma frequency

$$\omega_\mathrm{p} = \sqrt{\frac{e^2}{\epsilon_0}\frac{n_\uparrow + n_\downarrow}{m_\uparrow^* + m_\downarrow^*}}. \tag{9}$$

The effective masses m_σ^* are calculated via

$$\frac{m_\sigma^*}{m^0} = 1 - \left(\frac{\partial\,\mathrm{Re}\,G_{\boldsymbol{k}\sigma}^c(E_{\boldsymbol{k}\sigma}^c)}{\partial E_{\boldsymbol{k}\sigma}^c}\right)_{\varepsilon_{\boldsymbol{k}}} \tag{10}$$

at the Γ-point $\boldsymbol{k} = (000)$. In equation (8) $f_-(E) = [\exp(\frac{E-\mu}{k_\mathrm{B}T}) + 1]^{-1}$ denotes the Fermi function and in equation (10) $E_{\boldsymbol{k}\sigma}^c = \varepsilon_{\boldsymbol{k}} - \mu + \mathrm{Re}\,G_{\boldsymbol{k}\sigma}^c(E_{\boldsymbol{k}\sigma}^c)$ represent the quasiparticle resonance energies. The intrinsic effective mass $m^0 = (6\hbar^2)/(Wa^2)$ for $W = 3.5$ eV and $a = 5A$ equals half the free electron mass m_e.

2.4. Magnetic properties

For a consistent model study of the half-metals we are also interested in the magnetic properties. They are derived in the modified RKKY approach [11], where the Kondo-lattice Hamiltonian is mapped to an effective Heisenberg Hamiltonian and the magnetic properties are calculated self-consistently, using the single-electron Green functions. For the proposed two-band Kondo-lattice Hamiltonian (1) we will briefly recall the major steps in analogy to the derivation in [11].

The mapping of equation (1) to an effective Heisenberg Hamiltonian is achieved by averaging out the itinerant s-electron degrees of freedom, but retaining the operator character of the local-moment spin operators, yielding

$$H_\mathrm{sf} \to \langle H_\mathrm{sf}\rangle^{(s)} \equiv H_\mathrm{ff} = -\sum_{ij} J_{ij}^\mathrm{eff}\boldsymbol{S}_i \cdot \boldsymbol{S}_j. \tag{11}$$

In the averaging procedure the expectation value $\langle a_{\boldsymbol{k}+\boldsymbol{q}\sigma}^{b\dagger} a_{\boldsymbol{k}\sigma'}^b\rangle^{(s)}$ is calculated in the electronic subspace. This is achieved by the restricted Green function $G_{\boldsymbol{k}\sigma'\,\boldsymbol{k}+\boldsymbol{q}\sigma}^{b(s)}$, for which the equation of motion can be written down exactly. The iteration of the equation of motion was possible but would lead to higher orders of spin-operator products. Therefore, in the first iteration the single-electron Green functions (3) are used for decoupling. This leads to the effective Heisenberg exchange integrals as functionals of the Kondo-lattice single-electron Green functions

$$J_{ij}^\mathrm{eff} = \sum_b^{v,c}\left(\frac{1}{2}J^b\right)^2 \times \int f_-(E)\frac{1}{\pi}\,\mathrm{Im}\left(G_{ij0}^b(E)\sum_\sigma G_{ij\sigma}^b(E)\right)\mathrm{d}E. \tag{12}$$

The Green functions (3) are here used in their real space representation $G_{ij\sigma}^b(E) = N^{-1}\sum_{\boldsymbol{k}} G_{\boldsymbol{k}\sigma}^b(E)\mathrm{e}^{\mathrm{i}\boldsymbol{k}\cdot\boldsymbol{R}_{ij}}$ and $G_{ij0}^b(E)$ stands for the Green function of the free system ($J = 0$).

With the effective exchange integrals (12) the effective Heisenberg Hamiltonian (11) can now be used to calculate the magnetic properties in a standard procedure. We define a Green function of the local spin operators $\langle\langle S_i^+; \mathrm{e}^{aS_j^z}S_j^-\rangle\rangle$, whose equation of motion is decoupled using the Tyablikov approximation. With the Callen method [21] we eventually arrive at an equation for the mean magnetization

$$\langle S^z\rangle = \frac{(1+S+\varphi)\varphi^{2S+1} + (S-\varphi)(1+\varphi)^{2S+1}}{(1+\varphi)^{2S+1} - \varphi^{2S+1}}, \tag{13}$$

where $\varphi = N^{-1}\sum_{\boldsymbol{q}}[\exp(\frac{E(\boldsymbol{q})}{k_\mathrm{B}T}) - 1]^{-1}$ is the mean magnon number and $E(\boldsymbol{q}) = 2\langle S^z\rangle(J_{\boldsymbol{q}=0}^\mathrm{eff} - J_{\boldsymbol{q}}^\mathrm{eff})$ the magnon energies. The exchange integrals are used here in the reciprocal space representation $J_{\boldsymbol{q}}^\mathrm{eff} = N^{-1}\sum_{ij} J_{ij}^\mathrm{eff}\mathrm{e}^{-\mathrm{i}\boldsymbol{q}\cdot\boldsymbol{R}_{ij}}$.

Since the single-electron Green functions (3) are functionals of the mean magnetization (13) and vice versa, we get a closed system of equations which will be solved self-consistently. The results from those calculations are presented for one parameter set in the following section.

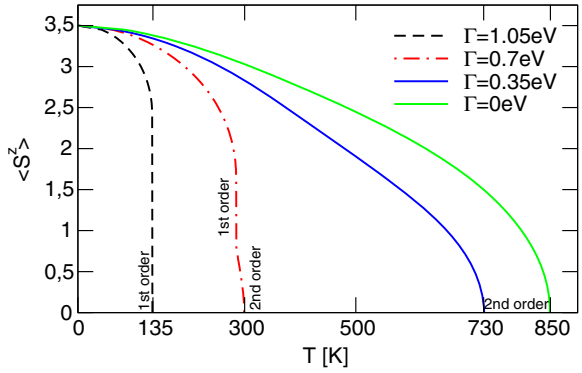

Figure 2. Temperature-dependent magnetization curves for different intrinsic band gaps Γ, fixed coupling strengths $J^c = -J^v = 0.5$ eV, band widths $W^c = W^v = 3.5$ eV and local spin quantum number $S = \frac{7}{2}$. The solid lines show second order phase transitions and the dashed line a first order phase transition at T_C. The intermediate regime is represented by the dash–dotted line which shows a first order phase transition close to T_C and one of second order at T_C. In the numerical calculations equation (13) was solved self-consistently, with the effective Heisenberg exchange integrals (12) and the electron Green functions (3).

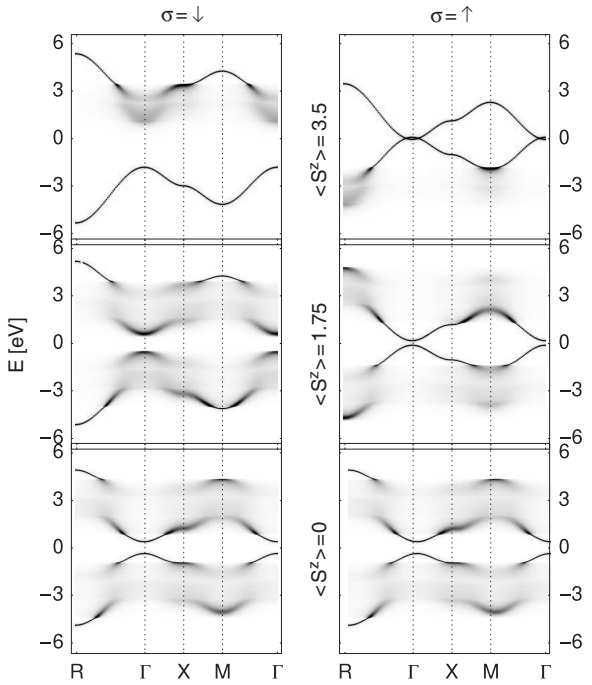

Figure 3. Bandstructure for ferromagnetic saturation at zero temperature (top), $\langle S^z \rangle = \frac{1}{2}S$ (middle) and in the paramagnetic state (bottom) (see footnote 1). The left-hand side shows the spin-down bandstructure, the right-hand side the spin-up one. The parameters are bandwidths $W^c = W^v = 3.5$ eV, intrinsic band gap $\Gamma = JS = 1.75$ eV, sf-coupling strengths $J^c = -J^v = 0.5$ eV and local spin quantum number $S = \frac{7}{2}$. The Fermi level lies at $\mu = 0$ eV. The spectral density is plotted as gray scale for wavevectors along the standard symmetry points of the first Brillouin zone for simple cubic lattices (equation (6)).

3. Results

The proposed two-band Kondo-lattice model (1) implies a strong mutual influence between the electronic and magnetic systems of the half-metals. On the one hand, the influence of the local magnetic moments on the itinerant carriers—electrons in the conduction band and holes in the valence band—leads to a magnetization-dependent band occupation. On the other hand, the magnetic exchange coupling via the itinerant carriers (modified RKKY; mRKKY) is a functional of the band occupation itself, thus is the mean magnetization. This mutual influence of the two subsystems is reflected in the different phase transitions which will be presented in this section.

For our qualitative description of ferromagnetic half-metals we will reduce the parameter space through setting the band widths of the valence and conduction bands to $W^v = W^c = 3.5$ eV, the local spin quantum number to $S = \frac{7}{2}$ and the exchange coupling strengths to $J^c = -J^v = 0.5$ eV. The variation of the intrinsic gap parameter Γ will shift the center of masses of the valence and conduction bands resulting in different regimes of band occupation, leading to the different behavior of the half-metals. We will vary the intrinsic gap as examples in the full range of possible ferromagnetism.

3.1. Magnetization

The magnetization curves in figure 2 have various shapes due to the dynamic band occupation. Two different regimes can be distinguished, namely those with magnetic phase transitions of first order (dashed line) and second order (solid lines). Furthermore, one parameter set (dash–dotted line) with a first order as well as second order phase transition is shown, representing the intermediate range. The critical exponents of the magnetization at the second order phase transitions at the Curie temperatures T_C are mean-field like ($\beta = 0.5 \pm 0.05$).

In all cases a band overlap exists at low temperatures and the itinerant carriers establish ferromagnetism. If, for increasing temperature, the carrier concentration becomes too low to maintain ferromagnetism via the RKKY mechanism, the magnetization drops down suddenly (first order phase transition, dashed line). If the carrier concentration is sufficient up to the Curie temperature, the phase transition is continuous (second order, solid lines). In the intermediate range (dash–dotted line) the carrier concentration in the bands is not big enough to hold up the RKKY mechanism above a temperature of 285 K, which leads to a sudden drop in the magnetization (first order transition). In contrast to the case with even lower band occupation (dashed line), the magnetization does not drop down to zero since the band occupation at temperatures between 285 and 300 K is sufficient to hold up a reduced magnetization. This leads to the second order phase transition at T_C.

In the next section we will have a closer look at how exactly the bandstructure changes under the variation of the net magnetization.

3.2. Bandstructure

The quasiparticle spectral density can be measured in (inverse) photoemission experiments. In figure 3 we plot the spin-dependent bandstructure as a gray scale of the spectral

density (6) at wavevectors along the standard symmetry points of the first Brillouin zone of simple cubic lattices. The degree of blackening is a measure of the height of the spectral density, and the width of the dispersion refers to the quasiparticle damping. A sharp deep-black line refers to long-living quasiparticles. The representation fits the bare line-shape of a respective (inverse) photoemission experiment. The bandstructure is presented for three different mean magnetizations which were fixed during the calculations[1]. The intrinsic gap $\Gamma = 1.75$ eV in figure 3 is chosen for easier discrimination between valence and conduction bands. For the intrinsic gap parameters used in figure 2 the bandstructures would look qualitatively the same as in figure 3, only the bands would be rigidly shifted towards each other by the difference in the intrinsic band gap.

Before we come to a detailed discussion of the dynamic band occupation, responsible for the different phase transitions, we will explain the general properties that can be seen from the bandstructures of the two-band Kondo-lattice model.

The upper right panel in figure 3 shows the two spin-up bands. The conduction band is the undeformed tight-binding band. At zero temperature the crystal is ferromagnetically saturated (all local-moments are aligned parallel). Thus no spin exchange processes between the spin-up conduction electrons and the local-moments are possible, and the band is only rigidly shifted by $-\frac{1}{2}JS$. The same holds for the spin-down valence band (top left panel), due to the more than half-filling of the valence band.

The faded regions in the bandstructure result from scattering processes of the electrons with the local-moments. Due to the scattering, the lifetime of those states is finite. In the sharp regions the spectral densities are delta functions and the quasiparticles have infinite lifetime. They cannot take part in spin exchange processes with the local-moments because no corresponding states with opposite spin are available. Instead one can think of virtual scattering for those states. At zero temperature the corresponding quasi particles are dressed by virtual clouds of magnons called magnetic polarons. This solution for the Kondo-lattice model can be found analytically and is part of the interpolating self-energy approach [19] used for equations (4) and (5).

With increasing temperature and decreasing magnetization (middle and lower panels), the bands almost split into two flattened sub-bands. The small overlap of spin-up valence and conduction bands decreases with temperature and turns into a considerable bandgap in the paramagnetic state (lower panels).

As already mentioned above for different intrinsic band gaps, like those in figure 2, the bands in figure 3 would be rigidly shifted towards each other resulting in greater band overlaps. The band overlap still changes with magnetization but varies in a different range. The different ranges are responsible for the different magnetization curves seen in figure 2 since the effective direct exchange coupling between the local-moments is mediated by the itinerant carriers (mRKKY mechanism).

For intrinsic band gaps of less than 0.7 eV the band occupation is sufficient to maintain the mRKKY mechanism in the whole temperature range. Thus the magnetization decreases continuously with increasing temperature, and the magnetic phase transition at the Curie temperature is of second order (solid lines in figure 2).

For intrinsic band gaps greater than 0.7 eV the band overlap that exists for large mean magnetizations vanishes while the magnetization decreases. Thus the band occupation goes to zero and the mRKKY mechanism cannot be upheld any longer. When reaching the critical temperature, the magnetization drops down suddenly and we see a first order magnetic phase transition (dashed lines in figure 2).

For intrinsic band gaps around 0.7 eV, the magnetization curve in figure 2 shows a first order as well as a second order phase transition. In this case the band overlap is sufficient to hold up a mean magnetization in the whole temperature range but it is not continuous. At the first critical temperature the magnetization drops down rapidly to continue at a smaller value continuously up to the Curie temperature.

3.3. Spin-polarization and electron density

The important property of half-metals is the spin polarization. In figure 4(a) we present the spin polarization P, calculated from equation (7) and in figure 4(b) the electron density $n = n_\uparrow + n_\downarrow$, from equation (8). The magnetization was calculated self-consistently as before.

One can see in the case $\Gamma = 1.05$ eV (first order magnetic phase transition) that the spin polarization and electron density drop down suddenly at T_C. Here, the sample undergoes a transition from half-metal to semiconductor.

For the cases $\Gamma < 0.7$ eV with second order magnetic phase transitions we have a smoothly decreasing spin polarization. These samples undergo a transition from half-metals to semimetals.

The case $\Gamma = 0.7$ eV, where a first and second order magnetic phase transition is present, shows a corresponding drop of electron density and spin-polarization at the same critical temperatures.

3.4. Plasma frequency

The plasma frequency can be obtained from optical absorption/reflectivity measurements. Figure 4(c) shows the plasma frequencies ω_p, calculated from equation (9) for the half-metals under discussion. It depends on the electron density as well as the effective mass, which both change with temperature in the introduced two-band Kondo-lattice model, although the electron density varies more compared to the effective mass. Thus, the variation of the plasma frequency mainly depends on the temperature-dependent electron density. Once more one can see the different behavior of the first and second order phase transitions as described above.

[1] The corresponding temperatures to the bandstructures in figure 3 can be read off from figure 2 (e.g. $\Gamma = 0.35$ eV the temperatures are 0 K, 530 K and 730 K).

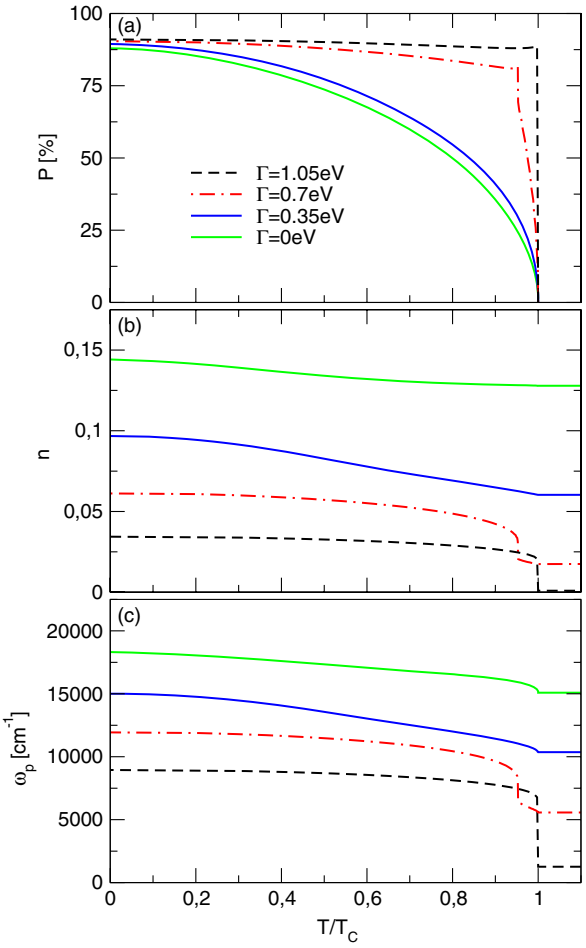

Figure 4. (a) Temperature-dependent spin-polarization P, (b) temperature-dependent electron density n and (c) temperature-dependent plasma frequency ω_p for different intrinsic band gaps Γ, fixed coupling strengths $J^c = -J^v = 0.5$ eV, band widths $W^c = W^v = 3.5$ eV and local spin quantum number $S = \frac{7}{2}$. The dashed line shows a transition from half-metal to semiconductor and the other lines from half-metal to semimetal.

4. Conclusion

We introduced a two-band Kondo-lattice model which describes valence and conduction electrons that are on-site coupled to local magnetic moments. By propagating through the lattice, the electrons are responsible for an effective direct exchange interaction (modified RKKY) between the local magnetic moments, which enables ferromagnetism.

The mutual influence between the spin-dependent band overlap of valence and conduction bands and the mean magnetization leads to different phase transitions. On the one hand it is possible to describe first as well as second order magnetic phase transitions. On the other hand one can explain the spin-electronic phase transitions: half-metal to semimetal and half-metal to semiconductor.

For future spintronic device applications one could think of two possible scenarios:

- We saw that changing the intrinsic bandgap would change the Curie temperatures and kinds of phase transitions. For example, applying hydrostatic pressure on a sample, thus changing the lattice constant in a small range and hence the intrinsic bandgap, could result in a variation of the electronic and magnetic properties. This would be especially interesting around the Curie temperature.
- A stronger impact on the sample would entail the application of an external magnetic field at temperatures around the Curie temperature. Depending on the specific properties of the sample, one can think of magnetic field-driven changes from the semiconducting (semimetallic) state to a half-metallic state.

In conclusion, first it is necessary to find appropriate materials for which the theory is suitable. The search for that should focus on compounds with the typical (ferromagnetic $J^c > 0$, antiferromagnetic $J^v < 0$) Kondo-lattice rare earths, such as Ce and Eu. Although the theory was developed for periodic crystals with local-moments on every lattice site, it is surely possible to expand the model to randomly distributed local-moment compounds, which should then show similar features. This possible future work would be interesting for the diluted magnetic semiconductors (DMS).

References

[1] Prinz G A 1998 *Science* **282** 1660
[2] de Groot R A, Mueller F M, van Engen P G and Buschow K H J 1983 *Phys. Rev. Lett.* **50** 2024
[3] de Groot R A and Buschow K H J 1986 *J. Magn. Magn. Mater.* **54–57** 1377
[4] Schwarz K-H 1986 *J. Phys. F: Met. Phys.* **16** L211
[5] Yanase A and Siratori K 1984 *J. Phys. Soc. Japan* **53** 312
[6] Park J H *et al* 1998 *Nature* **392** 794
[7] Galanakis I *et al* 2006 *J. Phys. D: Appl. Phys.* **39** 765
[8] Akai H 1998 *Phys. Rev. Lett.* **81** 3002
[9] Horne M *et al* 2004 *J. Phys.: Condens. Matter* **16** 5061
[10] Nolting W *et al* 1997 *J. Phys.: Condens. Matter* **9** 1301
[11] Santos C and Nolting W 2002 *Phys. Rev.* B **65** 1444419
[12] Skomski R 2007 *J. Phys.: Condens. Matter* **19** 315202
[13] Dagotto E, Yunoki S, Malvezzi A L, Moreo A, Hu J, Capponi S, Poilblanc D and Furukawa N 1998 *Phys. Rev.* B **58** 6414
[14] Yunoki S, Hu J, Malvezzi A L, Moreo A, Furukawa N and Dagotto E 1998 *Phys. Rev. Lett.* **80** 845
[15] Koller W, Prüll A, Evertz H G and von der Linden W 2003 *Phys. Rev.* B **67** 104432
[16] Peters R and Pruschke T 2007 *Preprint* 0707.0277v1
[17] Kreissl M and Nolting W 2005 *Phys. Rev.* B **72** 245117
[18] Jelitto R J 1969 *J. Phys. Chem. Solids* **30** 609
[19] Nolting W, Reddy G G, Ramakanth A and Meyer D 2001 *Phys. Rev.* B **64** 155109
[20] Nolting W, Reddy G G, Ramakanth A, Meyer D and Kienert J 2003 *Phys. Rev.* B **67** 024426
[21] Callen H B 1963 *Phys. Rev.* **130** 890